

Determining Shapes of Transparent Objects from Two Polarization Images

Daisuke Miyazaki Masataka Kagesawa Katsushi Ikeuchi
Institute of Industrial Science
The University of Tokyo *

Abstract

In the field of computer vision, beneficial methods of measuring surface shape of transparent objects such as glasses have rarely been proposed. In this paper, we propose a convenient and inexpensive method for measuring the surface shape of transparent objects. The degree of polarization of the light reflected from the object surface depends on the reflection angle which, in turn, depends on the object's surface normal; thus, by measuring the degree of polarization, we are able to calculate the surface normal of the object. But unfortunately, the relationship between degree of polarization and surface normal is not 1 to 1; thus, to obtain the true surface normal, we have to resolve this ambiguity problem. In this paper, we explain the method of resolving the ambiguity by using the differential-geometrical property of the object surface.

1 Introduction

In the field of computer vision, many methods which determine the surface shape of objects by vision systems have been developed[1, 8, 14]. Those methods mainly focus on opaque objects and do not focus on specular objects. Recently, researchers have enhanced these methods to measure the surface shape of specular objects. The stereo method has been extended to measure specular objects by Bhat[2] and Oren[18]. Photometric stereo, shape-from-shading and color photometric stereo have been improved to measure specular objects by Ikeuchi[9], Nayar[17], Hata[6] and Sato[22].

Zongker[27] and Chuang[5] have developed a method to synthesize a realistic image of transparent object without using any information about the 3D shape of the object. Schechner[23] and Szeliski[24] have separated the overlapped image of glass plates into two images; one is the reflected image, while the other is the transmitted image. Murase[16] have proposed a method to determine the surface shape of water wave by analyzing the image placed in the bottom of the water, which causes the image to be deformed due to refraction and undulation. Hata[7] have projected a light stripe onto transparent objects and recovered the surface shape of transparent objects by using a genetic algorithm.

Polarization has proven to be effective to estimate the shape of specular objects such as metals or transparent objects. Koshikawa[12, 13] analyzed the polarization of specular objects by illuminating the objects

with a circular polarized light to pick up, from the database, a 3D model of an object which matches the observed object. Wolff[25, 26] constrained the surface normal of the objects by analyzing the polarization of objects illuminated by unpolarized light. He also attempted to determine the surface shape of objects by using a combined method of polarization analysis and binocular stereo; however, he did not propose a method to search the corresponding points of two images; thus, he measured only the orientation of the glass plane and the metal plane. Saito[20, 21] tried to measure the surface shape of transparent objects; however, there was an ambiguity problem for determining the true surface normal, and she simply heuristically solved the ambiguity.

Miyazaki[15] extended Saito's method and solved the ambiguity problem from a polarization analysis of thermal radiation, and determined the surface shape of transparent objects. Rahmann[19] indicated that one can solve the corresponding problem in Wolff's method by the combined method of polarization analysis and trinocular stereo. However, this matching method is not a practical one, so he actually computed the surface shape of specular objects by the optimization method. He measured the surface shape of an opaque specular sphere by using polarization images taken from 5 directions.

In this paper, we propose a method to determine the surface shape of transparent objects by an easier way than those of Rahmann, Miyazaki and Hata. We solve the ambiguity problem of surface normal in Saito's method by rotating the object at a small angle. We solve the corresponding problem of binocular stereo in Wolff's method by using the geometrical property of the object surface. We do not need an extra infrared camera such as that used in Miyazaki's method. We do not require camera calibration, so we do not need to know the position of a projector as in Hata's method, and we do not need to know the rotation angle for stereo as in Rahmann's method. We use parabolic curves, where Gaussian curvature is 0, for searching the corresponding points[4, 8]. Parabolic curves are very important geometrical characteristics, and many well known researchers have investigated the application of this curve such as Klein, who invented the Klein bottle, and Koenderink[11].

We will describe the assumptions we require for our method in Section 2.

We will explain about the polarization analysis in Section 3. We will describe the ambiguity problem of surface normal: the relationship between the degree of polarization and the reflection angle is not one-to-one, and one cannot determine the true surface normal

*Address: 4-6-1 Komaba, Meguro-ku, Tokyo 153-8505 Japan.
E-mail: {miyazaki, kagesawa, ki}@cvl.iis.u-tokyo.ac.jp

unless one solves this ambiguity problem.

We solve the ambiguity problem by our proposed method described in Section 4. We will indicate the disambiguation method by introducing a binocular stereo method. Instead of setting two cameras, we rotate the object at a small angle. We compare two polarization images taken from two different directions: one polarization image is taken before the object is rotated and the other polarization image is taken after the object is rotated at a small angle. The degree of polarization must be compared at a couple of points which correspond to identical points on the object surface. We explain the corresponding method by analyzing the geometrical property on the object surface, which is invariant to the rotation of the object.

We present an experimental result in section 5, and suggest topics for our future work in Section 6.

2 Assumption

We assume an orthographic projection to the image plane of the camera. Target objects should comply with the following assumptions:

1. Object is transparent and solid
2. Refractive index is known
3. Surface is optically smooth (not rough)
4. Surface is geometrically smooth (C^2 surface)
5. Object is closed
6. No self-occlusion exists
7. Disambiguation method of azimuth angle ϕ shown in Section 3 can be applied
8. Object still obeys the above conditions even if we rotate the object at a small angle

From the seventh condition, several kinds of concave objects cannot be modeled automatically by our method.

The first condition is not necessary. Our method is also effective for opaque objects. The method can be applied only to perfect diffuse surfaces or to perfect specular surfaces; however, if we can separate the diffuse component and the specular component of the objects, we can apply our method to any objects.

In addition to above assumptions, our method assumes that there are no interreflections and the rotation angle of the object is infinitesimal. However, interreflections actually occur, and the interference of interreflections can be changed by rotating the object at a large angle. If the rotation angle is too small, the difference of obtained data will be small, and computing the shape will be difficult. Actually, there are more interreflections in transparent objects than in opaque objects. Now, according to our way of thinking, a method which can measure the shape of transparent objects is robustly applicable to any other objects. Thus, to prove the robustness of our method, we applied our method to transparent objects.

3 DOP and reflection angle

In this section, we describe the relationship between the degree of polarization (DOP) and the reflection angle. Details are described in [3, 15, 20, 21, 25, 26].

Geometrical location of the acquisition system is shown in Figure 1. We locate the camera over the target object, and locate the polarizer in front of the

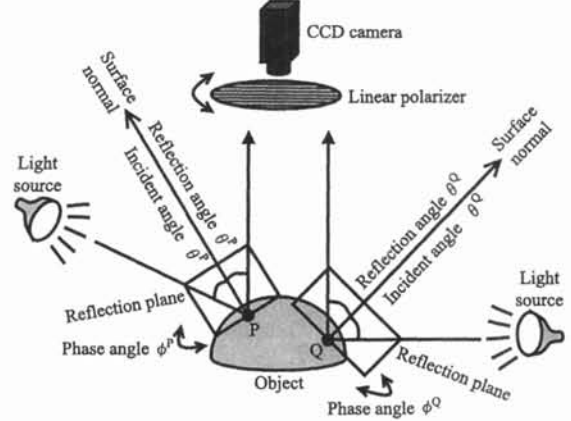


Figure 1: Location of acquisition system

camera. We illuminate the object with unpolarized light traveling through the air where the refractive index is 1.0. Unpolarized light will become partially polarized light if the light reflects from the object surface where the refractive index is n . We observe such reflected light. The angle between the light source direction and the surface normal is called the incident angle, and the angle between the surface normal and the camera direction is called the reflection angle. The incident angle is equal to the reflection angle for optically smooth transparent objects. The plane consisting of the surface normal and the camera direction is called the reflection plane. Consider projecting the reflection plane onto the image plane: the reflection plane appears to be a straight line on the image plane, and the orientation of this line is called a phase angle.

Surface normal can be represented by zenith angle θ and azimuth angle ϕ . Reflection angle (= incident angle) corresponds to zenith angle, and phase angle corresponds to azimuth angle. Two phase angles are calculated in the range of $0 \leq \phi < 360^\circ$, and the difference of those two angles is 180° . Since we know the surface normal is heading vertically to the viewing direction at the occluding boundary, we can solve the ambiguity problem of the phase angle by propagating the determined phase angle from the occluding boundary to the inner part of the object region. Therefore, we have only to determine the reflection angle in order to obtain the surface normal of the object surface.

We rotate the polarizer and observe the object by the camera and calculate the DOP. DOP of reflected light ranges from 0 to 1: DOP is 0 for unpolarized light, and DOP is 1 for perfectly polarized light. The following formula represents the relationship between DOP and the reflection angle [15, 20, 21].

$$\rho = \frac{2 \sin^2 \theta \cos \theta \sqrt{n^2 - \sin^2 \theta}}{n^2 - \sin^2 \theta - n^2 \sin^2 \theta + 2 \sin^4 \theta} \quad (1)$$

DOP ρ is a function of refractive index n and reflection angle θ . We assume that the refractive index is given. We can compute the reflection angle from the DOP.

Figure 2 represents equation (1). The vertical axis represents the DOP, and the horizontal axis represents the reflection angle. If the reflection angle is 0° or 90° , then the DOP will be 0; and if the reflection angle is

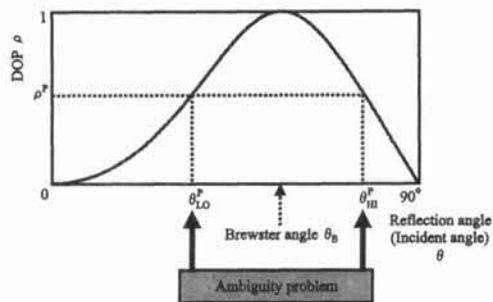


Figure 2: Relation between DOP and reflection angle



Figure 3: Photo of bell-shaped acrylic object

Brewster angle, θ_B , then the DOP will be 1. We obtain two reflection angles from one DOP, except for the Brewster angle. One of the angles is the true reflection angle and the other is not. We have to solve this ambiguity problem to determine the true surface normal, and we describe the disambiguation method in Section 4.

4 Disambiguation

4.1 Brewster segmentation

We obtain the DOP values of whole points over the object surface, and we call those obtained DOP values the DOP image. Obtained DOP image of the object shown in figure 3 is shown in figure 4(a). Figure 3 is a photo of a bell-shaped transparent object. The DOP is represented as a gray image in figure 4(a), where white represents 0 DOP and black represents 1 DOP.

We divide the DOP image into some regions whose boundaries will be the points of Brewster angle, namely, the points where the DOP is 1. We call the closed curve which consists of only Brewster angle the Brewster curve. We call this region segmen-

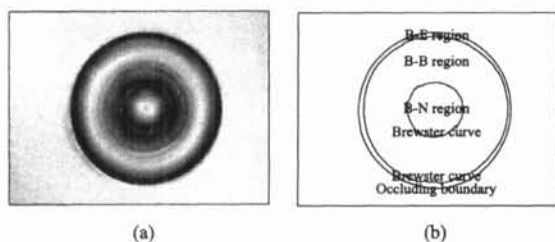


Figure 4: (a) DOP image and (b) result of Brewster segmentation, of bell-shaped acrylic object

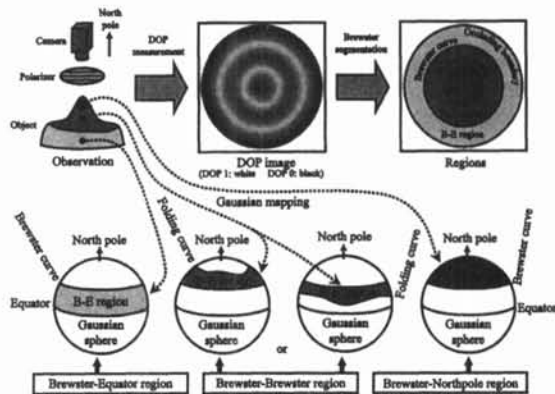


Figure 5: Gaussian mapping and regions

tation Brewster segmentation. We disambiguate each region after the Brewster segmentation. Since we assume the object to be a closed smooth object, we can disambiguate whole points in a certain region if we disambiguate only one point in the region.

Figure 4(b) is the result of Brewster segmentation computed from the DOP image of figure 4(a). There are two Brewster curves and one occluding boundary in figure 4(b).

We classify each region into 3 types (figure 5):

1. B-E region
2. B-N region
3. B-B region

B is for Brewster, N is for North Pole, and E is for Equator. There is one B-E region, B-N region, B-B region each in figure 4(b).

We define the B-E region as a region that includes an occluding boundary. Consider a Gaussian sphere (unit sphere) where the north pole is directed toward the camera, and correspond the points of the B-E region onto this sphere by Gaussian mapping. The occluding boundary will be mapped onto the equator of the Gaussian sphere. Points on the equator will satisfy $\theta = 90^\circ$. We can disambiguate the points of B-E region as $\theta_B \leq \theta < 90^\circ$. Occluding boundary is calculated by background subtraction.

We define B-N region as a region including a point where $\theta = 0^\circ$. Points where $\theta = 0^\circ$ will be mapped onto the north pole of Gaussian sphere. We assume that there is no self-occlusion even if we rotate the object at a small angle: if there is a point where $\rho = 0$ in the region, and still there is a point where $\rho = 0$ in the region even if we rotate the object at a small angle, we know that such point is not $\theta = 90^\circ$ but $\theta = 0^\circ$. Thus, we can disambiguate the points of B-N region as $0^\circ \leq \theta \leq \theta_B$.

Disambiguation of the points of B-B region is more difficult than that of B-E region and B-N region. We will explain the disambiguation method of B-B region in the following sections.

4.2 Folding curve

Now, we rotate the object against the camera at a small angle (figure 6). We solve the ambiguity problem by comparing DOP images taken both before and after rotation.

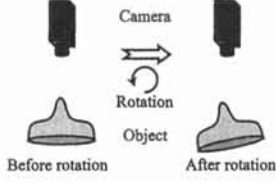


Figure 6: Rotate the object at a small angle

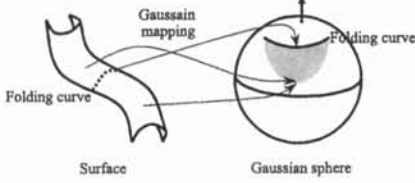


Figure 7: Gaussian mapping of bell-shaped surface

Two DOP values must be compared at an identical point on the object surface. We have to search for two points, one point in each DOP images where geometrical properties of the object surface coincide.

Figure 5 represents the Gaussian mapping of regions from object surface to the Gaussian sphere. The north pole of the Gaussian sphere represents the camera position, as we have suggested previously. B-B region on the object surface is enclosed only by the Brewster curve, and does not include the points where $\theta = 0^\circ$ or $\theta = 90^\circ$; thus, B-B region on the Gaussian sphere does not include the north pole or the equator. Since the object surface is smooth, a closed region on the object surface maps onto a closed region even on Gaussian sphere. Thus, B-B region on Gaussian sphere is always enclosed by a Brewster curve and additional curves. We define such a curve, which is not a Brewster curve, as a folding curve *or* a global folding curve.

Consider the Gaussian mapping shown in figure 7 to discuss the characteristics of the folding curve. The figure represents the Gaussian mapping of a part of a bell-shaped surface. The dotted curve on the surface described in the figure corresponds to a curve on the Gaussian sphere described in the figure, and this curve will be a folding curve. Note that the points of the surface map only onto one side of the folding curve.

Consider mapping a local part of a surface onto a Gaussian sphere; if points of the surface map only onto one side of a curve on the Gaussian sphere and do not map onto the other side of such curve, we define such curve as a folding curve *or* a local folding curve.

Theorem 1 *A folding curve is a parabolic curve (= a curve whose Gaussian curvature is 0).*

(Proof) This proof is explained with figure 8. Figure 8(a) represents an object surface, and figure 8(b) represents a Gaussian sphere that corresponds to figure 8(a). Vertical curves depicted in these figures represent folding curves. We locate p and r on the folding curve of the object surface. We also locate s on one side of the folding curve, and q on the other side of the folding curve. p , q , r and s are located separately and do not overlap on another. We denote the points on the Gaussian sphere as, p' , q' , r' , s' , which correspond

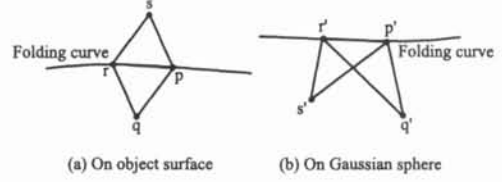


Figure 8: (a) Folding curve and 4 points on object surface, (b) folding curve and 4 points on Gaussian sphere mapped from (a)

to the points on the object surface, p , q , r , s . p' and r' will be located on the folding curve of the Gaussian sphere. From the definition of a local folding curve, q' and s' map onto the same side of a folding curve.

The area of triangle prq , psr , and $p'r'q'$ will become positive; however, the area of triangle $p's'r'$ becomes negative. Gaussian curvature K of p can be calculated from the limit taken by approaching q , r and s to p .

$$K = \lim_{r, q \rightarrow p} \frac{\Delta p'r'q'}{\Delta prq} \geq 0 \quad (2)$$

$$K = \lim_{s, r \rightarrow p} \frac{\Delta p's'r'}{\Delta psr} \leq 0 \quad (3)$$

As a result, Gaussian curvature K at p will be 0.

Even if the location of p' and r' is the opposite location to that shown in figure 8(b), namely, even if p' is located to the left and r' is located to the right, we can also give a proof that is the same as this proof. Even if p or r is not a curve but a surface, we can also give a proof similar to this proof. In the case of $p' = r'$, $p' = q'$, $p' = s'$, $r' = q'$, $r' = s'$ or $q' = s'$, we can give a proof more easily than this proof. \square

From the above arguments, we conclude that the folding curve is a geometrical characteristic invariant to object rotation.

Consider a great circle which represents the rotation direction. We call this great circle the rotation circle. The rotation circle includes the two poles. Points that correspond to the rotation circle still correspond to the rotation circle after the object rotation. Surface normal of the points on the rotation circle is parallel to the rotation direction. We define the intersection of the rotation circle and the global folding curve of B-B region as the corresponding point. From figure 9, we realize that the corresponding point is a point which has minimum DOP within the points in B-B region where the surface normal is parallel to the rotation direction. We can prove such nature of the corresponding point from the definition of rotation circle, global folding curve, and from the unimodality of function (1); however, we will not describe the proof. We first execute Brewster segmentation to the obtained two DOP images, and then we search for one corresponding point in each B-B region.

Figure 10 represents the Gaussian mapping of a surface resembling a children's slide. The dotted curve on the surface shown in the figure maps onto only one point on the Gaussian sphere; this point is a folding point. Since more than one point of the surface map onto one point on the Gaussian sphere, it is very difficult to correspond one point to one point on the surface. However, this is not an important matter, since

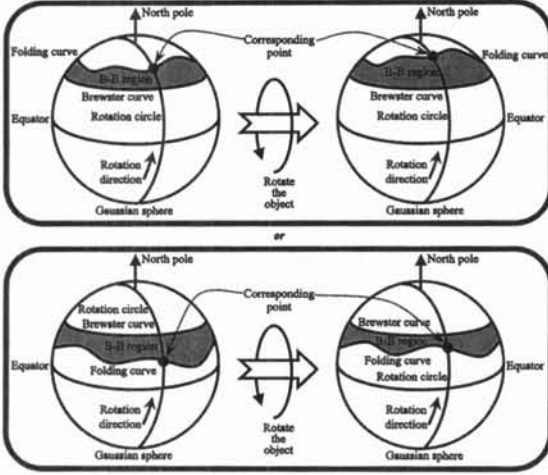


Figure 9: Corresponding point

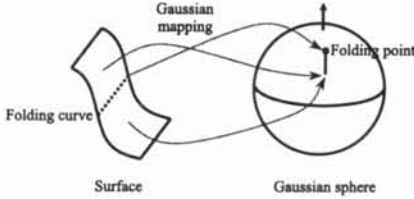


Figure 10: Gaussian mapping of slide-shaped surface

we need only the value of the DOP at the corresponding point: points that map onto one point on the Gaussian sphere have the same DOP. Note that most other researchers use the notation “corresponding point” as the point on an object surface; however, we define the “corresponding point” as a point on the Gaussian sphere rather than on the object surface.

4.3 Difference of DOP

Now, we denote the DOP of the object before rotation as $\rho(\theta)$, and denote the DOP of the object rotated at a small angle $\Delta\theta$ as $\rho(\theta + \Delta\theta)$. Then, the difference of the DOP at a couple of corresponding points will be as follows.

$$\rho(\theta + \Delta\theta) - \rho(\theta) \simeq \rho'(\theta)\Delta\theta \quad (4)$$

The graph of DOP ρ is shown in figure 11(a), and the graph of the derivative of DOP ρ' is shown in figure 11(b).

The derivative of the DOP is positive when $0^\circ < \theta < \theta_B$, and negative when $\theta_B < \theta \leq 90^\circ$. We assume that the rotation direction is given, namely, the sign of $\Delta\theta$ is given. The sign of the difference of the DOP at corresponding points can be calculated from obtained DOP images. Thus, from equation (4), we can determine whether the points of the region satisfy $0^\circ < \theta < \theta_B$ or $\theta_B < \theta \leq 90^\circ$; namely, we can solve the ambiguity problem. Note that there is no ambiguity problem for a point where $\theta = \theta_B$, and there is no point where $\theta = 0^\circ$ in B-B region.

Our proposed method uses only the sign for disambiguation, not the value. Thus the method is robust,

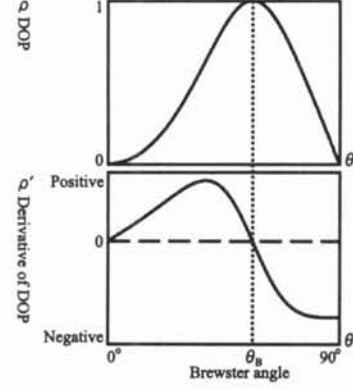


Figure 11: Derivative of DOP

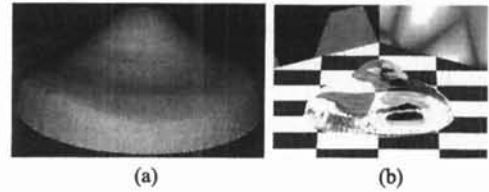


Figure 12: Obtained shape: (a) shading image, (b) raytracing image

and we do not need to know the rotation angle, which is an absolute value of $\Delta\theta$. Since we do not need to know the rotation angle, we do not need camera calibration. Even if there was an error in DOP value or even if the rotation angle was not so small, the sign of DOP would rarely change. The method is robust; thus, even if we do not give a precise rotation direction, there is no difficulty for disambiguation.

5 Result

We employed the same acquisition system as [15, 20, 21]. We obtained DOP images of the object surface by this acquisition system, computed the surface normal of object surface, and finally integrated the surface normal data to the height data by using relaxation method [8, 10].

We applied our method to the object shown in figure 3, and the result is shown in figure 12. The target object was a bell-shaped acrylic object where the refractive index is 1.5 and the diameter(width) is 24mm. We computed the whole surface shape of the object by our method. The rendered images are shown in figure 12: figure 12(a) is an example of shading image, figure 12(b) is an example of raytracing result.

Figure 13 represents the shape of the object observed from the side view. The obtained shape is represented as dotted curve, and the true shape is represented as solid curve. Note that we artificially created the true shape by hand from the silhouette of the photo taken from the side of the target object. According to the figure, the height error was calculated to be approximately 0.4mm.



Figure 13: Obtained height and true height

6 Future work

We are now developing a method which works more precisely than this method. Error is mainly caused by interreflection of transparent objects. We have to consider the influence of not only the top surface (= visible surface) of the object but also the bottom surface (= occluded surface) of the object.

We should also improve the method for determining the phase angle. If such a method is developed, we will be able to measure any concave objects. However, concave objects cause strong interreflections; thus, we have to develop a method which can deal with the interreflections.

Consequently, our future work is to develop a method which can handle the influence of interreflection.

References

- [1] Ballard, D.H. and Brown, C.M.: *Computer Vision*, Prentice-Hall (1982).
- [2] Bhat, D.N. and Nayar, S.K.: Stereo and Specular Reflection, *Intl. J. Computer Vision*, Vol. 26, No. 2, pp. 91-106 (1998).
- [3] Born, M. and Wolf, E.: *Principles of Optics*, Pergamon Press (1959).
- [4] do Carmo, M.P.: *Differential Geometry of Curves and Surfaces*, Prentice-Hall (1976).
- [5] Chuang, Y., Zongker, D.E., Hindorff, J., Curless, B., Salesin, D.H. and Szeliski, R.: Environment Matting Extensions: Towards Higher Accuracy and Real-time Capture, *Proc. SIGGRAPH 2000*, New Orleans, Louisiana, pp. 121-130 (2000).
- [6] Hata, S.: Shape Detection of Small Specular Surface using Color Stripe Lighting, *Proc. Intl. Conf. Pattern Recognition*, The Hague, The Netherlands, pp. I:554-557 (1992).
- [7] Hata, S., Saitoh, Y., Kumamura, S. and Kaida, K.: Shape Extraction of Transparent Object using Genetic Algorithm, *Proc. Intl. Conf. Pattern Recognition*, Vienna, Austria, pp. 684-688 (1996).
- [8] Horn, B.K.P.: *Robot Vision*, MIT Press (1986).
- [9] Ikeuchi, K.: Determining Surface Orientations of Specular Surfaces by Using the Photometric Stereo Method, *IEEE Trans. Pattern Analysis and Machine Intelligence*, Vol. 3, No. 6, pp. 661-669 (1981).
- [10] Ikeuchi, K.: Reconstructing a Depth Map from Intensity Maps, *Proc. Intl. Conf. Pattern Recognition*, Montreal, Canada, pp. 736-738 (1984).
- [11] Koenderink, J.J.: *Solid Shape*, MIT Press (1990).
- [12] Koshikawa, K.: A Polarimetric Approach to Shape Understanding of Glossy Objects, *Proc. Intl. Joint Conference on Artificial Intelligence*, Tokyo, Japan, pp. 493-495 (1979).
- [13] Koshikawa, K. and Shirai, Y.: A Model-based Recognition of Glossy Objects using their Polarimetric Properties, *Advances in Robotics*, Vol. 2, No. 2, pp. 137-147 (1987).
- [14] Marr, D.: *Vision: A Computational Investigation into the Human Representation and Processing of Visual Information*, W.H. Freeman (1982).
- [15] Miyazaki, D., Saito, M., Sato, Y. and Ikeuchi, K.: Determining Surface Orientations of Transparent Objects Based on Polarization Degrees in Visible and Infrared Wavelengths, *J. Optical Society of America A*, Vol. 19, No. 4, pp. 687-694 (2002).
- [16] Murase, H.: Surface Shape Reconstruction of an Undulating Transparent Object, *Proc. IEEE Intl. Conf. Computer Vision*, Osaka, Japan, pp. 313-317 (1990).
- [17] Nayar, S.K., Ikeuchi, K. and Kanade, T.: Determining Shape and Reflectance of Hybrid Surface by Photometric Sampling, *IEEE Trans. Robotics and Automation*, Vol. 6, No. 4, pp. 418-431 (1990).
- [18] Oren, M. and Nayar, S.K.: A Theory of Specular Surface Geometry, *Intl. J. Computer Vision*, Vol. 24, No. 2, pp. 105-124 (1997).
- [19] Rahmann, S. and Canterakis, N.: Reconstruction of Specular Surfaces using Polarization Imaging, *Proc. IEEE Conf. Computer Vision and Pattern Recognition*, Kauai Marriott, Hawaii, pp. I:149-155 (2001).
- [20] Saito, M., Sato, Y., Ikeuchi, K. and Kashiwagi, H.: Measurement of Surface Orientations of Transparent Objects using Polarization in Highlight, *Proc. IEEE Conf. Computer Vision and Pattern Recognition*, Fort Collins, Colorado, pp. 381-386 (1999).
- [21] Saito, M., Sato, Y., Ikeuchi, K. and Kashiwagi, H.: Measurement of Surface Orientations of Transparent Objects by use of Polarization in Highlight, *J. Optical Society of America A*, Vol. 16, No. 9, pp. 2286-2293 (1999).
- [22] Sato, Y. and Ikeuchi, K.: Temporal-color Space Analysis of Reflection, *J. Optical Society of America A*, Vol. 11, No. 11, pp. 2990-3002 (1994).
- [23] Schechner, Y., Shamir, J. and Kiryuati, N.: Polarization-based Decorrelation of Transparent Layers: The Inclination Angle of an Invisible Surface, *Proc. IEEE Intl. Conf. Computer Vision*, Corfu, Greece, pp. 814-819 (1999).
- [24] Szeliski, R., Avidan, S. and Anandan, P.: Layer Extraction from Multiple Images Containing Reflections and Transparency, *Proc. IEEE Conf. Computer Vision and Pattern Recognition*, Hilton Head Island, South Carolina, pp. 246-253 (2000).
- [25] Wolff, L.B.: Polarization-based Material Classification from Specular Reflection, *IEEE Trans. Pattern Analysis and Machine Intelligence*, Vol. 12, No. 11, pp. 1059-1071 (1990).
- [26] Wolff, L.B. and Boulton, T.E.: Constraining Object Features Using a Polarization Reflectance Model, *IEEE Trans. Pattern Analysis and Machine Intelligence*, Vol. 13, No. 7, pp. 635-657 (1991).
- [27] Zongker, D.E., Warner, D.M., Curless, B. and Salesin, D.H.: Environmental Matting and Compositing, *Proc. SIGGRAPH 99*, Los Angeles, California, pp. 205-214 (1999).